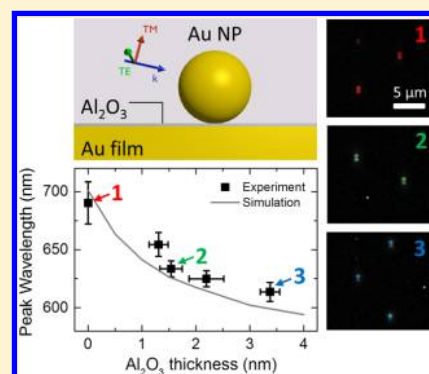Article

Wide-Band Spectral Control of Au Nanoparticle Plasmon Resonances on a Thermally and Chemically Robust Sensing Platform

Chatdanai Lumdee,[†] Binfeng Yun,[‡] and Pieter G. Kik*,[†,§]

[†]CREOL, The College of Optics and Photonics, University of Central Florida, 4000 Central Florida Blvd., Orlando, Florida 32816, United States

[‡]Advanced Photonics Center, School of Electronic Science and Engineering, Southeast University, Nanjing 210096, China

S *Supporting Information*

ABSTRACT: Gold nanoparticles on Al_2O_3-coated gold films are presented as a chemically and thermally robust platform for molecular sensing. Single particle spectroscopy as a function of Al_2O_3 coating thickness shows reproducible gold nanoparticle scattering spectra in the range from 690 to 610 nm as the Al_2O_3 thickness increases from 0 to 3.4 nm. Numerical simulation of these structures indicates that surface-enhanced Raman spectroscopy enhancement factors in excess of 10^6 can be achieved. The stability of the Al_2O_3-coated structures under high-power laser irradiation was tested, revealing stable scattering spectra upon irradiation with 100 W/mm² at the particle resonance wavelength. The presented structure solves challenges with thermal stability, wavelength tuning range, and Raman background signal associated with previously attempted approaches.

1. INTRODUCTION

Plasmonic resonances of metal nanostructures are widely used in sensing applications due to the extremely strong localized field enhancement they can produce, enabling the sensitive detection of analyte molecules in ultrasmall volumes through changes in plasmon resonance wavelength, fluorescence signal strength, and Raman scattering signal. Plasmon-mediated field enhancement has enabled single-molecule Raman spectroscopy in small metal nanoparticle aggregates.[1,2] The main enabling element in these experiments is the formation of nanogaps between adjacent nanoparticles, resulting in *hot spots*: regions that exhibit extremely high field enhancement factors. While particle aggregates produce large field enhancement, the randomness of the structure formation and the extreme sensitivity of the optical response to the gap size make nanoaggregates unpredictable, unstable, and difficult to produce reliably. For these reasons, a lot of effort has been put into developing plasmon-mediated biochemical sensor platforms that can provide small gap sizes while also having predictable and stable plasmon resonances. Select approaches include the use of electron-beam lithography (EBL),[3,4] on-wire lithography,[5,6] and self-assembly.[7–9]

An approach that has recently been receiving increasing attention is the use of chemically synthesized metal nanoparticles deposited onto high dielectric constant substrates or onto metallic films with an optional spacer layer. In the resulting structures, a hot spot is formed in the gap between the nanoparticle and the substrate due to the development of dynamic image charges in the substrate.[10–12] This approach allows the controlled formation of structures that provide high field enhancement using low-cost and simple fabrication methods.[13,14] Moreover, this approach can make use of nanostructures that are close to their thermodynamic equilibrium shape (approximately spherical), promising thermally stable performance. Finally, the plasmon resonance wavelengths of supported nanoparticles can be controlled by modifying the nanoparticle-to-substrate separation, e.g., using a low-dielectric constant spacer layer on a large dielectric constant substrate. Using this approach, it has been shown that plasmon resonances of gold nanoparticles which typically occur in the green can be tuned across the entire visible range by changing the substrate composition,[11,15] modifying the substrate thickness,[16] and adjusting the gap size between the nanoparticle and the substrate.[17–20] These approaches move the plasmon resonance of stable Au nanospheres to frequencies well below Au interband transitions, resulting in sharper plasmon resonances and larger field enhancement factors. Prior demonstrations of substrate-controlled plasmon resonance made use of organic spacer layers,[17,21] which when used in Raman detection are expected to introduce a background signal due to Raman scattering from the spacer layer molecules and may be chemically or thermally damaged relatively easily. An alternate approach using all-inorganic materials resulted in fragile systems[19] due to weak oxide−substrate binding using the SiO_2−Au system or a limited tuning range[20] due to the presence of a native oxide layer using the Al_2O_3−Al system.

To address these issues, here we present experiments on the control of the plasmon resonance of Au nanoparticles using
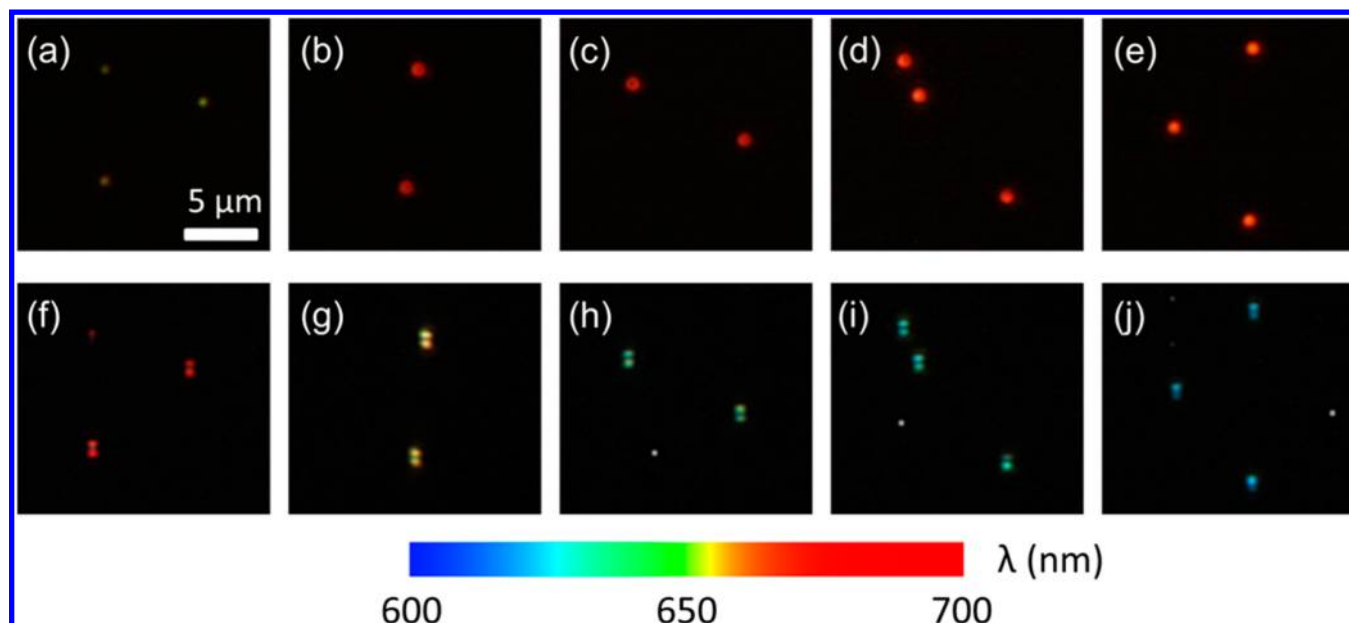
Figure 1. (a−e) Real-color dark-field microscopy images of gold nanoparticles on gold substrates with Al_2O_3 coating thickness 0, 1.3, 1.5, 2.2, and 3.4 nm, respectively. (f−j) False-color images of these same nanoparticles obtained using a hyperspectral camera taken in the range 500−800 nm. The color bar shows the wavelength representation used in parts f−j.

aluminum oxide (Al_2O_3)-coated gold films experimentally and numerically. We demonstrate that this structure provides reproducible Au nanoparticle resonance spectra that can be spectrally tuned over at least an 80 nm bandwidth by varying the oxide spacer thickness and that remain virtually unaltered upon high-power laser irradiation. The controllable and reproducible plasmon resonance wavelength, large tuning range, stability of the structure under laser irradiation, and the chemical stability of all materials used make the presented system a good candidate for a reliable plasmonic sensing platform for applications such as surface-enhanced Raman spectroscopy (SERS) and plasmon-enhanced fluorescence spectroscopy.[22−24]

2. EXPERIMENTAL SECTION

Sample Preparation and Characterization. Aluminum oxide-coated gold films were prepared by thermal evaporation using a multipocket Edwards FL 400 thermal evaporator (base pressure <10^{-5} mbar). Gold films with a thickness of 50 ± 2 nm were deposited onto glass coverslips using a 2 nm Cr wetting layer. Few-nanometer-thick aluminum films were deposited onto the gold-coated samples without breaking vacuum. A gold substrate without Al coating was used as a reference sample. The film thickness of all deposited films was verified using a Woollam M2000 variable angle spectroscopic ellipsometer. Al films are well-known to form a thin native surface oxide layer of 2−4 nm[25] upon exposure to ambient environment. The Al layers deposited in the experiment are thinner than the 3.6 nm Al_2O_3 thickness formed on thermal-evaporated Al films[20] and completely oxidized into a thin Al_2O_3 layer after exposure to air. Indeed, no evidence of metallic aluminum was found in postdeposition variable angle spectroscopic ellipsometry. Long-range Al_2O_3 thickness variation on each sample was verified by performing ellipsometry at various locations on the samples. The variations in the measured thickness are included as error bars in Figure 4. The root-mean-square surface roughness of the samples was determined using atomic force microscopy (AFM). The roughness was found to be ~1.5 nm on samples with and without Al_2O_3 coating, indicating that the roughness is dominated by the Au film roughness. Following the deposition steps, a colloidal solution of gold nanoparticles (BBInternational) with a batch-specific size distribution of 60.4 ± 2.6 nm was diluted in ethanol to a concentration of 2×10^8 particles/ mL and drop-coated onto the substrates. The droplet was observed to spread rapidly across the sample surface and was subsequently left to dry in air. Postdeposition microscopy of the samples revealed well-separated optical scatterers attributed to the presence of isolated Au nanoparticles, with interparticle separations exceeding several micrometers. A large-area dark-field microscopy image of the resulting scatterers on a gold film is provided in the Supporting Information (Figure S1).

Optical Microscopy and Spectroscopy. Dark-field microscopy images were taken using an Olympus IX-71 inverted microscope equipped with a 50× dark-field objective (Olympus UMPlanFL 50× BD, N.A.= 0.75) and a Canon EOS 450D digital camera. Spectral images of the samples were recorded using a HSi-440C Hyperspectral Imaging System (Gooch & Housego) at a spectral resolution of 10 nm. Scattering spectra of individual gold nanoparticles were collected using an imaging spectrometer attached to the microscope (Horiba iHR320 with Synapse CCD array) with an effective collection area of ~$8 \times 8 \ \mu m^2$ at the sample surface and a spectral resolution of 10 nm. All spectra were corrected for the dark current and normalized to the scattering spectrum of a nearby region of the sample.

Numerical Simulation and Calculation. Numerical simulations were done based on the frequency domain finite integration technique[26] using literature data for the dielectric functions of gold[27] and aluminum oxide,[28] as described in detail in the Supporting Information.

Single Particle Stability Measurements. A linearly polarized 633 nm laser beam was focused onto the substrate at an angle of incidence of 15° using off-center illumination of

the back aperture of a 50× dark-field objective. The beam polarization was chosen to result in p-polarized irradiation of the Au nanoparticles. The laser spot was found to be close to circular with an approximately Gaussian beam profile and a fwhm of ~2.2 μm as measured by nanoparticle-mediated beam sampling (see Supporting Information). The peak irradiance incident on the nanoparticles was set to ~100 W/mm^2.

3. RESULTS AND DISCUSSION

Dark-Field Microscopy and Single Particle Spectroscopy. Dark-field microscopy images of gold nanoparticles on Al$_2$O$_3$-coated gold films with five different Al$_2$O$_3$ thicknesses (0, 1.31 ± 0.18, 1.54 ± 0.21, 2.20 ± 0.32, and 3.37 ± 0.18 nm) were recorded by two CCD cameras: a Canon EOS 450D digital camera for real-color images and a HSi-440C Hyperspectral Imaging System for spectral images. Figures 1a–e show representative real-color dark-field microscopy images of isolated gold nanoparticles on five samples. Figure 1a shows the scattering observed from three Au nanoparticles. The particles appear green, with each particle exhibiting a single central maximum of the scattering intensity. This kind of spot shape is known to be indicative of a laterally (surface-parallel) polarized charge oscillation on the particle.[29,30] In addition the green spots are seen to be surrounded by a faint red ring-shaped scattering pattern. This spot shape is indicative of a z-polarized (vertically polarized) plasmon resonance and has been observed previously on metal nanoparticles on various metallic substrates.[18,20,29] Figures 1b–e show similar images taken of samples with a progressively thicker Al$_2$O$_3$ layer between the Au nanoparticle and the gold film. All images show a similar red ring-shaped scattering pattern, while the green central spot appears relatively weak. These images seem to suggest that the spectral differences among the four Al$_2$O$_3$-coated samples are limited. Figures 1f–j show corresponding false-color images of the same particles shown in Figures 1a–e, based on images taken with a hyperspectral camera attached to the microscope. Images were taken in the spectral range 500–800 nm with a collection bandwidth of 10 nm per image, and a spectral sampling of 3 nm, resulting in a stack of 100 images. The images were processed as described in the Supporting Information, resulting in a color mapping of the peak scattering wavelength according to the scale bar shown below the images. Figure 1f shows the false color image of the same three Au nanoparticles on the gold film shown in Figure 1a. Two main differences are observed. First, the central maximum (green scattering signal in Figure 1a) is not visible since the false-color mapping emphasizes wavelengths in the range 600–700 nm. Second, instead of a ring-shaped scattering image, two separated scattering spots are observed. This is a result of the polarization sensitive nature of the hyperspectral imager, eliminating the left and right parts of the ring-shaped pattern. Figures 1f–j reveal that the red z-polarized plasmon resonance is gradually tuned toward shorter wavelengths as the Al$_2$O$_3$ thickness increases. Additionally, particles in each individual spectral image appear of the same color, showing that a consistent resonance wavelength is obtained at each oxide thickness. These assertions are corroborated by additional single particle scattering spectra presented below.

To evaluate the response of the nanoparticles in Figure 1 in more detail, a large set of single-particle scattering spectra were taken for each sample. Figure 2a shows a typical scattering spectrum of an isolated gold nanoparticle on the gold substrate without Al$_2$O$_3$ (black solid line). The gray region represents the
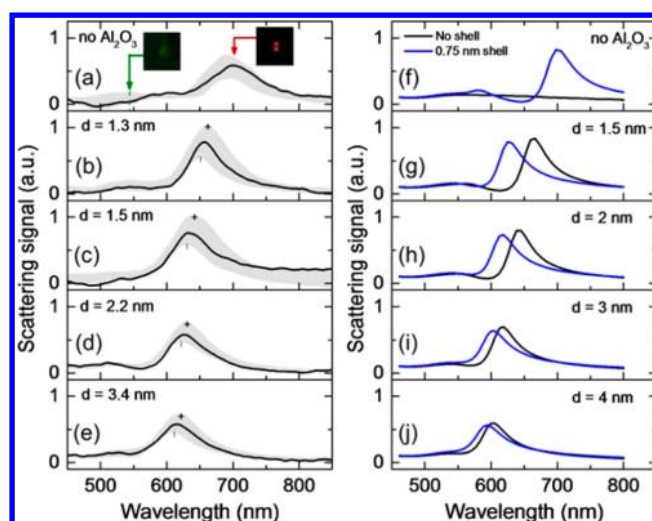

Figure 2. (a–e) Measured scattering spectra from single gold nanoparticles on gold substrates without an Al$_2$O$_3$ spacer layer and with 1.3, 1.5, 2.2, and 3.4 nm Al$_2$O$_3$ spacer layer, respectively. The shaded region on each plot represents the confidence intervals of the measurement, and the black curve shows a typical scattering spectrum. The green arrow indicates the plasmon resonance wavelength of gold nanoparticles in colloidal solution. The insets in (a) show spectral images obtained from the same particle by collecting wavelength bands 545–555 nm and 695–705 nm. (f–j) Calculated scattering spectra of 60 nm gold nanoparticles on gold films coated with 0, 1.5, 2, 3, and 4 nm of Al$_2$O$_3$, respectively. The blue curves in (f–j) show the simulated scattering spectra assuming the presence of a 0.75 nm thick organic shell on the gold nanoparticle.

one-sigma confidence interval obtained by taking spectral measurements of 15 randomly selected particles on the same sample. The spectrum shows a plasmon enhanced scattering peak at a wavelength of 690 nm (1.775 eV), with a full width at half-maximum (fwhm) of 88 nm (0.223 eV). The observed spectral shape and line width are typical for a dipolar plasmon resonance in gold nanoparticles and similar to the extinction peak width of these gold nanoparticles in colloidal solution (~80 nm line width). However, the resonance wavelength is red-shifted by ~150 nm compared to the plasmon resonance wavelength of 544 nm of these nanoparticles in colloidal solution (green dashed line and arrow in Figure 2a). The measured spectra also contain weak scattering features around 500–550 nm. The insets of Figure 2a show spectral images obtained from the same particle by collecting wavelength bands 545–555 nm (left) and 695–705 nm (right). These images confirm that the signal between 500 and 550 nm originates from an at least partly laterally polarized green plasmon resonance, while the signal at 690 nm originates from a z-polarized red plasmon resonance. The large red-shift of the z-polarized resonance results from an interaction between the z-polarized electric dipole of the nanoparticle and induced dynamic image charges in the substrate.[20,31,32] The observed variation in signal strength of the scattering spectra as indicated by the confidence interval is attributed to the specified size variation of ±2.6 nm of the nanoparticles leading to an anticipated variation of the scattering signal strength by as much as ~30% assuming a scattering cross section that is proportional to the square of the particle volume.[33] Note that the relatively strong scattering strength of the z-polarized resonance seems at odds with the observation of the weak red scattering in Figure 1a. This is a result of the infrared cut filter

present in the camera, leading to reduced response at wavelengths larger than 600 nm.

Figures 2b−e show the corresponding typical spectra and confidence intervals for gold nanoparticles on gold films coated with 1.3 nm (24 particles), 1.5 nm (14 particles), 2.2 nm (22 particles), and 3.4 nm (20 particles) thick Al_2O_3 spacer layers, respectively. As the oxide thickness increases from 0 to 3.4 nm, the peak scattering wavelength is seen to blue-shift from 690 to 610 nm. This observed tuning range of 80 nm is significantly larger than that observed using anodization of an Al substrate in ref 20, where a resonance shift of only ∼30 nm was observed. The larger tuning range is made possible by the absence of a limiting native oxide thickness, which allows for smaller particle−substrate separations than can be achieved in an Al_2O_3-coated Al system exposed to air. The scattering spectra of gold nanoparticles located directly on the gold film (Figure 2a) are seen to be broader than those of gold nanoparticles on Al_2O_3-coated substrates (Figures 2b−e), exhibiting line widths of ∼80 and 50−60 nm, respectively. This may be due to the increased importance of nonlocal effects on the Au response for small particle-substrate spacing.[34,35] Note that the scattering peak height of the z-polarized mode varies by less than 17% as the oxide thickness is changed (one-sigma interval). Finally, note that for all Al_2O_3-coated samples the lower bound of the confidence interval (marked by a vertical dash) peaks at a shorter wavelength than the upper bound of the confidence interval (marked by a plus symbol). This observation corroborates the assertion that the observed brightness fluctuations are due to particle size variations, since larger nanoparticles are known to produce stronger scattering signal and longer resonance wavelength; see e.g. Supporting Information of ref 20.

Numerical Simulation and Calculated Scattering Spectrum. To understand the observations made in Figures 1 and 2a−e, numerical simulations were carried out (see Supporting Information). Figure 2f presents the simulated scattering spectrum of a 60 nm diameter gold nanoparticle on a 50 nm gold film on a glass substrate with a refractive index of 1.5 (black line). The simulated spectrum shows a broad and weak scattering band around 550 nm and no evidence of a long wavelength resonance, markedly different from the experimentally observed spectrum. Part of this difference may be due to the fact that the simulation does not take into account the expected presence of organic ligands that remain on the particle surface or the Au film surface after deposition from solution. The simulations were repeated assuming that the nanoparticle surface is covered with a 0.75 nm thick organic layer, corresponding to the thickness of a monolayer of normally oriented citrate molecules. This choice results in a spectrum (Figure 2f, blue line) that closely resembles the experimental data, showing a clear peak at 697 nm and a weaker scattering peak at 580 nm.

Figures 2g−j show the simulated scattering spectra of 60 nm diameter gold nanoparticles on gold films coated with a 1.5, 2, 3, and 4 nm thick Al_2O_3 layer. The figures contain both the calculated spectra of gold nanoparticle with and without a 0.75 nm organic coating. Both sets of the spectra show the same general trend as observed experimentally although it is clear that the presence of organic ligands significantly blue-shifts the spectral response of the particle.

To clarify the nature of the observed resonances, Figure 3 shows the calculated scattering spectrum of an Au nanoparticle on the Au film, assuming the presence of a 0.75 nm organic
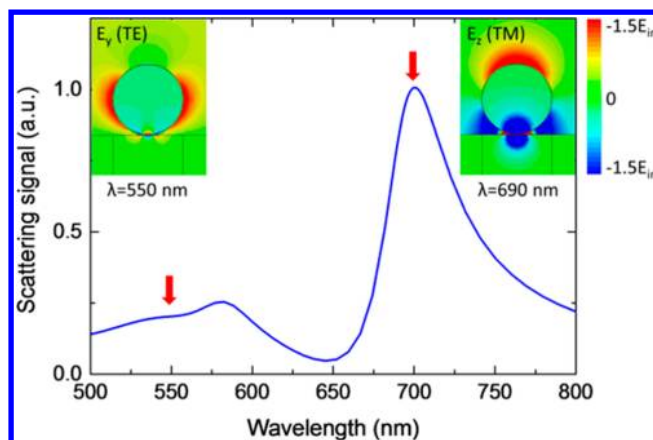

Figure 3. Calculated scattering spectrum of a 60 nm diameter Au nanoparticle coated with a 0.75 nm thick organic shell on a gold film. Insets show corresponding electric field snapshots at 550 and 690 nm under TE and TM illumination, respectively, shown on the same relative scale.

coating on the particle. The insets show electric field snapshots in the (x,z) plane of E_y (lateral field) at the green resonance (550 nm) under TE illumination and of E_z (normal field) at the red resonance (690 nm) under TM illumination, displayed on the same relative scale. The full color range represents a maximum magnitude of 1.5 times the incident field strength. The lateral field distribution at the green resonance shows moderate field enhancement throughout the particle responsible for part of the observed scattering signal. The normal (z-polarized) field distribution at the red resonance, on the other hand, shows a predominantly dipolar mode with a large electric field in the gap between the nanoparticle and the gold substrate. The secondary peak at 575 nm is the result of a higher order plasmon resonance of the nanoparticle with a net z-polarized dipole moment (see Supporting Information).

Figure 4a summarizes the measured scattering peak wavelengths as a function of the Al_2O_3 thickness based on ∼100 measured single-particle scattering spectra, as well as the
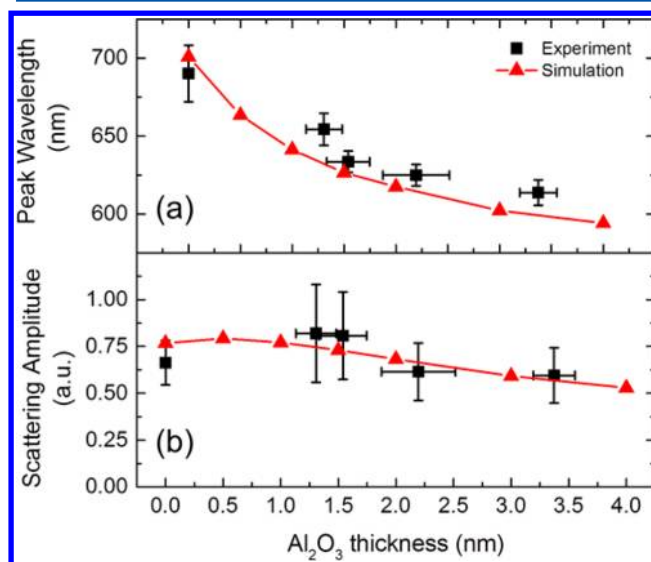

Figure 4. Measured (black squares) and simulated (red triangles) scattering peak wavelength (a) and peak intensity (b) of single gold nanoparticles on a gold film with different Al_2O_3 coating thicknesses.

corresponding simulated data. The measured data (black squares) and the simulated data for nanoparticles coated with a 0.75 nm organic ligand layer (red triangles) show a similar dependence on spacer layer thickness. Figure 4b presents the corresponding data sets for the relative peak scattering signal of the gold nanoparticles on each substrate. The measured scattering intensity exhibits relatively little variation as the spacer layer thickness is changed. This relative insensitivity of the scattering signal strength to the spacer layer thickness is reproduced in the simulations, both with and without the assumed presence of an organic coating on the nanoparticles.

To evaluate the applicability of these structures to SERS-based detection of molecules on the particle surface, the enhancement of the surface-normal electric field E_z relative to the z-component of the incident field $E_{z,inc}$ was determined underneath the particle inside the 0.75 nm thick organic shell. The peak field enhancement factors $E_{z,peak}/E_{z,inc}$ range from ~441 to ~39 for the limiting cases of 0 nm Al_2O_3 and 4 nm Al_2O_3, respectively, corresponding to predicted SERS enhancement factors $|E_{z,peak}|^4/|E_{z,inc}|^4$ ranging from 3.8×10^{10} to 2.4×10^6. This expression for the SERS enhancement factor assumes that the detected Raman shifts are much smaller than the plasmon line width.[36,37] These calculations do not take into account effects of nonlocality that are expected to reduce the field enhancement factors at small gap sizes. In addition, the listed enhancement factors would change if the particle shape changes, e.g., when the incident laser power exceeds the damage threshold of the irradiated structures. The particle stability against laser irradiation will be investigated in the following section. Note that the use of an inorganic spacer layer as done in the experiments has the added anticipated advantage that the support itself does not add Raman lines typical of organic molecular bonds, and consequently it is expected that the current structure allows for SERS measurements with relatively low Raman background signal.

Single Particle Scattering Stability. Given the extreme sensitivity of the spectral position of the nanoparticle resonances to structural changes on the subnanometer scale, it must be verified whether these structures remain stable under typical measurement conditions in laser-excited spectroscopy such as SERS. To test the stability of the structures under laser irradiation, isolated nanoparticles were exposed to laser powers 2 orders of magnitude higher than those typically used in SERS of ~1 W/mm², and scattering spectra of the same nanoparticle were obtained before and after laser irradiation to verify spectral stability. A linearly polarized 633 nm laser beam was focused onto the substrate with the peak irradiance incident on the nanoparticles ~100 W/mm² for all subsequent measurements. The beam polarization was chosen to result in p-polarized irradiation of the Au nanoparticles, necessary for achieving the large gap-fields associated with the z-polarized resonance. Note that the laser wavelength is close to the z-polarized resonance wavelengths experimentally observed in this study.

Figure 5a shows scattering spectra of a gold nanoparticle on the gold substrate without Al_2O_3 coating before and after laser irradiation for 1 min shown on the same relative scale. A significant change in the scattering spectrum is observed. Both the short and long wavelength resonance shift significantly, and the brightness of the long wavelength peak is seen to reduce substantially. The experiment was repeated several times on separate particles, with similarly large spectral changes observed in all cases. Notably, the scattering spectra of these particles were found to be different after each successive irradiation,
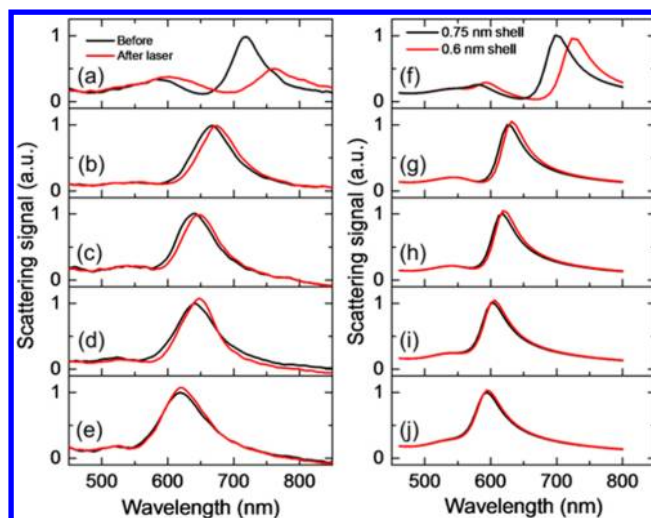

Figure 5. (a−e) Normalized scattering spectra of single gold nanoparticles on gold films coated with 0, 1.3, 1.5, 2.2, and 3.4 nm Al_2O_3 layers, respectively. The red and black curves represent the spectra before and after 1 min of laser illumination at ~100 W/mm², respectively. (f−j) Calculated scattering spectra of gold nanoparticles with a 0.75 nm (black line) and 0.6 nm (red line) organic shell on gold films with 0, 1.5, 2, 3, and 4 nm Al_2O_3 coating, respectively. The black and red dashed lines in (f) correspond to the same particle with a 0.6 and 0.5 nm organic coating, respectively.

indicating that no stable equilibrium particle configuration was reached. Figure 5b presents the scattering spectrum of a gold nanoparticle on an Al_2O_3 coated gold substrate with a 1.3 nm Al_2O_3 thickness before and after laser irradiation. Contrary to the observations in Figure 5a, the nanoparticle on the thin Al_2O_3 coating shows a relatively stable scattering spectrum. Irradiation is only seen to introduce a small (<10 nm) red-shift of the spectrum and a slight (<8%) increase in the peak scattering intensity. Similarly small changes in the scattering spectra were found in samples with 1.5, 2.2, and 3.4 nm thick Al_2O_3 coatings, as shown in Figures 5c−e, respectively. In contrast with the observations made for particles in the absence of an Al_2O_3 coating, the spectra in Figures 5b−e remain stable after prolonged irradiation.

The remarkable stability of Au nanoparticles on Al_2O_3-coated Au films under high power laser irradiation is attributed to their close proximity to their equilibrium thermodynamic shape as well as the stability of the oxide spacer layer used. Given the subtle nature of the spectral changes observed in Figure 5, it seems unlikely that the observed spectral shifts are the result of any major changes in the nanoparticle shape. One possible origin of the small spectral shifts is the slight modification of the particle−substrate interaction. To investigate this possibility, scattering spectra were calculated of a gold nanoparticle on the same Al_2O_3 spacer layers as in Figure 2 with a 0.75 nm organic shell and a 0.6 nm organic shell on the nanoparticle (black and red solid lines respectively). These simulations should be considered illustrations of the effect of subnanometer changes in the effective particle−substrate separation, e.g., through slight nanoparticle deformation, changes in configuration or position of any remaining organic ligands on the Au nanoparticle surface, or the thermally stimulated removal of organic molecules from the gap region. The possibility of the thermally induced temporary removal of a surface water layer was rejected, since the red-shift persisted for minutes after the irradiation. Figures 5g−j show the simulated spectra for the

Al_2O_3 supported Au nanoparticle with different organic shell thicknesses. For each Al_2O_3 spacer layer thickness a similar effect is observed: the reduction of the organic layer thickness 1.5 Å results in a small red-shift of the resonance peak. These simulated resonance shifts are slightly smaller than those observed in the corresponding experimental images (Figures 5b−e). Intriguingly another experimentally observed trend is reproduced remarkably well by the simulations: the experiments show that the peak scattering wavelength becomes less sensitive to laser irradiation on samples with a thicker Al_2O_3 spacer layer. This trend is reproduced in the numerical simulations while assuming an identical structural change in all cases (here represented by a 1.5 Å reduction in the organic cover layer thickness). This trend can be understood by noting that the distance dependence of the plasmon resonance becomes less pronounced at large spacer layer thickness, as observed in Figure 4a. These observations support the assumption that the laser-induced spectral changes are related to small changes in particle−substrate interaction. Please note that the presented data indicate the stability against irradiation of gold nanoparticles on an Al_2O_3-coated gold substrate; however, note that analyte molecules may decompose or otherwise be modified at lower irradiation powers.

Despite the good correspondence between experimental and simulated trends in Figure 5 for Al_2O_3-coated samples, significant differences are observed for the sample not coated with Al_2O_3. The results obtained with the 1.5 Å reduction in organic shell thickness show a smaller reduction in peak scattering signal and a smaller red-shift than observed experimentally. The differences are possibly due to the fact that the numerical simulations ignore nonlocal effects[34,35,38] or effects related to electron tunneling expected to occur at small gap sizes.[39−41]

Several alternative hypotheses were considered to explain the observed spectral shifts observed upon laser irradiation, including significant thermally induced changes in particle shape (faceting), the formation of a finite electrically conductive contact area between particle and substrate in the case of an Au nanoparticle on the Au film, and the development of the theoretically expected contact angle of Au on Al_2O_3 upon laser irradiation. However, none of the corresponding numerical simulations led to satisfactory agreement in spectral shape and spectral location, leading to e.g. dramatically larger red-shifts or the development of pronounced multipolar resonances that were not observed experimentally. The irradiances used here are also substantially lower than those used in recent work that demonstrated particle deformation due to optical gradient forces (~100 times).[42] We therefore conclude that the spectral changes observed here are due to minute changes in effective particle−substrate interaction, possible due to redistribution, deformation, oxidation, or removal of surface molecular layers.

4. CONCLUSION

In conclusion, we demonstrate wide-band plasmon resonance tuning of gold nanoparticles on thermally and chemically stable Al_2O_3-coated gold substrates. Dark-field microscopy images and hyperspectral images show well-separated scattering patterns indicative of a strong z-polarized plasmon resonance. Optical spectroscopy of individual nanoparticles shows spectral tuning from 690 to 610 nm as the Al_2O_3 thickness increases from 0 to 3.4 nm. The observed tuning range of ~80 nm is 3 times larger than previously achieved for Au nanoparticle resonances tuned with anodized Al substrates, as the current structure does not

suffer from a limiting native oxide layer thickness. Simulated scattering spectra show a good agreement with experimental observations, and the corresponding field enhancement factors suggest SERS enhancement factors well in excess of 10^6 are possible. The scattering spectra on Al_2O_3 coated Au films were found to remain stable upon prolonged exposure to 100 W/mm^2 laser illumination near the nanoparticle plasmon resonance wavelength, demonstrating that this structure may be used as a reliable optical biochemical sensing platform.

■ ASSOCIATED CONTENT

ⓢ Supporting Information

The method used for generating a false color image from a stack of spectral images, the finite integration technique based simulation model and the calculation process for obtaining single particle scattering spectra, and the laser spot size measurement by nanoparticle-mediated beam sampling. This material is available free of charge via the Internet at http://pubs.acs.org.

■ AUTHOR INFORMATION

Corresponding Author

*E-mail: kik@creol.ucf.edu (P.G.K.).

Notes

The authors declare no competing financial interest.
§Also with Physics Department, University of Central Florida, 4000 Central Florida Blvd, Orlando, FL 32816.

■ ACKNOWLEDGMENTS

■ REFERENCES

(1) Kneipp, K.; Wang, Y.; Kneipp, H.; Perelman, L. T.; Itzkan, I.; Dasari, R.; Feld, M. S. Single Molecule Detection Using Surface-Enhanced Raman Scattering (SERS). *Phys. Rev. Lett.* **1997**, *78*, 1667−1670.

(2) Nie, S. M.; Emery, S. R. Probing Single Molecules and Single Nanoparticles by Surface-Enhanced Raman Scattering. *Science* **1997**, *275*, 1102−1106.

(3) Xia, Y. N.; Halas, N. J. Shape-Controlled Synthesis and Surface Plasmonic Properties of Metallic Nanostructures. *MRS Bull.* **2005**, *30*, 338−344.

(4) Elechiguerra, J. L.; Reyes-Gasga, J.; Yacaman, M. J. The Role of Twinning in Shape Evolution of Anisotropic Noble Metal Nanostructures. *J. Mater. Chem.* **2006**, *16*, 3906−3919.

(5) Qin, L. D.; Park, S.; Huang, L.; Mirkin, C. A. On-Wire Lithography. *Science* **2005**, *309*, 113−115.

(6) Osberg, K. D.; Rycenga, M.; Harris, N.; Schmucker, A. L.; Langille, M. R.; Schatz, G. C.; Mirkin, C. A. Dispersible Gold Nanorod Dimers with Sub-5 Nm Gaps as Local Amplifiers for Surface-Enhanced Raman Scattering. *Nano Lett.* **2012**, *12*, 3828−3832.

(7) Haynes, C. L.; Van Duyne, R. P. Nanosphere Lithography: A Versatile Nanofabrication Tool for Studies of Size-Dependent Nanoparticle Optics. *J. Phys. Chem. B* **2001**, *105*, 5599−5611.

(8) Tran, M. L.; Centeno, S. P.; Hutchison, J. A.; Engelkamp, H.; Liang, D.; Van Tendeloo, G.; Sels, B. F.; Hofkens, J.; Uji-i, H. Control of Surface Plasmon Localization Via Self-Assembly of Silver Nano-

particles Along Silver Nanowires. *J. Am. Chem. Soc.* **2008**, *130*, 17240−17241.

(9) Lim, D. K.; Jeon, K. S.; Kim, H. M.; Nam, J. M.; Suh, Y. D. Nanogap-Engineerable Raman-Active Nanodumbbells for Single-Molecule Detection. *Nat. Mater.* **2010**, *9*, 60−67.

(10) Nordlander, P.; Prodan, E. Plasmon Hybridization in Nanoparticles near Metallic Surfaces. *Nano Lett.* **2004**, *4*, 2209−2213.

(11) Knight, M. W.; Wu, Y. P.; Lassiter, J. B.; Nordlander, P.; Halas, N. J. Substrates Matter: Influence of an Adjacent Dielectric on an Individual Plasmonic Nanoparticle. *Nano Lett.* **2009**, *9*, 2188−2192.

(12) Lei, D. Y.; Fernandez-Dominguez, A. I.; Sonnefraud, Y.; Appavoo, K.; Haglund, R. F.; Pendry, J. B.; Maier, S. A. Revealing Plasmonic Gap Modes in Particle-on-Film Systems Using Dark-Field Spectroscopy. *ACS Nano* **2012**, *6*, 1380−1386.

(13) Hill, R. T.; Mock, J. J.; Urzhumov, Y.; Sebba, D. S.; Oldenburg, S. J.; Chen, S. Y.; Lazarides, A. A.; Chilkoti, A.; Smith, D. R. Leveraging Nanoscale Plasmonic Modes to Achieve Reproducible Enhancement of Light. *Nano Lett.* **2010**, *10*, 4150−4154.

(14) Mubeen, S.; Zhang, S. P.; Kim, N.; Lee, S.; Kramer, S.; Xu, H. X.; Moskovits, M. Plasmonic Properties of Gold Nanoparticles Separated from a Gold Mirror by an Ultrathin Oxide. *Nano Lett.* **2012**, *12*, 2088−2094.

(15) Chen, S. Y.; Mock, J. J.; Hill, R. T.; Chilkoti, A.; Smith, D. R.; Lazarides, A. A. Gold Nanoparticles on Polarizable Surfaces as Raman Scattering Antennas. *ACS Nano* **2010**, *4*, 6535−6546.

(16) Le, F.; Lwin, N. Z.; Steele, J. M.; Kall, M.; Halas, N. J.; Nordlander, P. Plasmons in the Metallic Nanoparticle - Film System as a Tunable Impurity Problem. *Nano Lett.* **2005**, *5*, 2009−2013.

(17) Jiang, G. Q.; Baba, A.; Ikarashi, H.; Xu, R. S.; Locklin, J.; Kashif, K. R.; Shinbo, K.; Kato, K.; Kaneko, F.; Advincula, R. Signal Enhancement and Tuning of Surface Plasmon Resonance in Au Nanoparticle/Polyelectrolyte Ultrathin Films. *J. Phys. Chem. C* **2007**, *111*, 18687−18694.

(18) Mock, J. J.; Hill, R. T.; Degiron, A.; Zauscher, S.; Chilkoti, A.; Smith, D. R. Distance-Dependent Plasmon Resonant Coupling between a Gold Nanoparticle and Gold Film. *Nano Lett.* **2008**, *8*, 2245−2252.

(19) Hu, M.; Ghoshal, A.; Marquez, M.; Kik, P. G. Single Particle Spectroscopy Study of Metal-Film-Induced Tuning of Silver Nanoparticle Plasmon Resonances. *J. Phys. Chem. C* **2010**, *114*, 7509−7514.

(20) Lumdee, C.; Toroghi, S.; Kik, P. G. Post-Fabrication Voltage Controlled Resonance Tuning of Nanoscale Plasmonic Antennas. *ACS Nano* **2012**, *6*, 6301−6307.

(21) Mock, J. J.; Hill, R. T.; Tsai, Y. J.; Chilkoti, A.; Smith, D. R. Probing Dynamically Tunable Localized Surface Plasmon Resonances of Film-Coupled Nanoparticles by Evanescent Wave Excitation. *Nano Lett.* **2012**, *12*, 1757−1764.

(22) Muskens, O. L.; Giannini, V.; Sanchez-Gil, J. A.; Rivas, J. G. Strong Enhancement of the Radiative Decay Rate of Emitters by Single Plasmonic Nanoantennas. *Nano Lett.* **2007**, *7*, 2871−2875.

(23) Bek, A.; Jansen, R.; Ringler, M.; Mayilo, S.; Klar, T. A.; Feldmann, J. Fluorescence Enhancement in Hot Spots of Afm-Designed Gold Nanoparticle Sandwiches. *Nano Lett.* **2008**, *8*, 485−490.

(24) Fu, Y.; Zhang, J.; Lakowicz, J. R. Largely Enhanced Single-Molecule Fluorescence in Plasmonic Nanogaps Formed by Hybrid Silver Nanostructures. *Langmuir* **2013**, *29*, 2731−2738.

(25) Gulbransen, E. A.; Wysong, W. S. Thin Oxide Films on Aluminum. *J. Phys. Colloid Chem.* **1947**, *51*, 1087−1103.

(26) *Cst Microwave Studio*, Computer Simulation Technology, Darmstadt, Germany, 2012.

(27) Johnson, P. B.; Christy, R. W. Optical Constants of the Noble Metals. *Phys. Rev. B* **1972**, *6*, 4370−4379.

(28) Lichtenstein, T. *Handbook of Thin Film Materials*; University of Rochester: New York, 1979.

(29) Chen, H. J.; Ming, T.; Zhang, S. R.; Jin, Z.; Yang, B. C.; Wang, J. F. Effect of the Dielectric Properties of Substrates on the Scattering Patterns of Gold Nanorods. *ACS Nano* **2011**, *5*, 4865−4877.

(30) King, N. S.; Li, Y.; Ayala-Orozco, C.; Brannan, T.; Nordlander, P.; Halas, N. J. Angle- and Spectral-Dependent Light Scattering from Plasmonic Nanocups. *ACS Nano* **2011**, *5*, 7254−7262.

(31) Takemori, T.; Inoue, M.; Ohtaka, K. Optical-Response of a Sphere Coupled to a Metal-Substrate. *J. Phys. Soc. Jpn.* **1987**, *56*, 1587−1602.

(32) Ruppin, R. Optical-Absorption by a Small Sphere above a Substrate with Inclusion of Nonlocal Effects. *Phys. Rev. B* **1992**, *45*, 11209−11215.

(33) Bohren, C. F.; Huffman, D. R. *Absorption and Scattering of Light by Small Particles*; Wiley: New York, 1983.

(34) David, C.; de Abajo, F. J. G. Spatial Nonlocality in the Optical Response of Metal Nanoparticles. *J. Phys. Chem. C* **2011**, *115*, 19470−19475.

(35) Ciraci, C.; Hill, R. T.; Mock, J. J.; Urzhumov, Y.; Fernandez-Dominguez, A. I.; Maier, S. A.; Pendry, J. B.; Chilkoti, A.; Smith, D. R. Probing the Ultimate Limits of Plasmonic Enhancement. *Science* **2012**, *337*, 1072−1074.

(36) Stiles, P. L.; Dieringer, J. A.; Shah, N. C.; Van Duyne, R. R. Surface-Enhanced Raman Spectroscopy. *Annu. Rev. Anal. Chem.* **2008**, *1*, 601−626.

(37) Le Ru, E. C.; Etchegoin, P. G. Rigorous Justification of the [E] (4) Enhancement Factor in Surface Enhanced Raman Spectroscopy. *Chem. Phys. Lett.* **2006**, *423*, 63−66.

(38) de Abajo, F. J. G. Nonlocal Effects in the Plasmons of Strongly Interacting Nanoparticles, Dimers, and Waveguides. *J. Phys. Chem. C* **2008**, *112*, 17983−17987.

(39) Mao, L.; Li, Z. P.; Wu, B.; Xu, H. X. Effects of Quantum Tunneling in Metal Nanogap on Surface-Enhanced Raman Scattering. *Appl. Phys. Lett.* **2009**, *94*, 243102.1−243102.3.

(40) Zuloaga, J.; Prodan, E.; Nordlander, P. Quantum Description of the Plasmon Resonances of a Nanoparticle Dimer. *Nano Lett.* **2009**, *9*, 887−891.

(41) Esteban, R.; Borisov, A. G.; Nordlander, P.; Aizpurua, J. Bridging Quantum and Classical Plasmonics with a Quantum-Corrected Model. *Nat. Commun.* **2012**, *3*, 825.1−825.9.

(42) Kuhlicke, A.; Schietinger, S.; Matyssek, C.; Busch, K.; Benson, O. In Situ Observation of Plasmon Tuning in a Single Gold Nanoparticle during Controlled Melting. *Nano Lett.* **2013**, *13*, 2041−2046.